



ELSEVIER

Contents lists available at ScienceDirect

## Journal of Physics and Chemistry of Solids

journal homepage: [www.elsevier.com/locate/jpcs](http://www.elsevier.com/locate/jpcs)

## Measurement of Seebeck effect (thermoelectric power) at high pressure up to 40 GPa

Vladimir V. Shchennikov<sup>a</sup>, Sergey V. Ovsyannikov<sup>a,b,c,\*</sup>, Andrei Y. Manakov<sup>d</sup><sup>a</sup> High Pressure Group, Institute of Metal Physics of Russian Academy of Sciences, Urals Division, 18S. Kovalevskaya Str., GSP-170, Yekaterinburg 620041, Russia<sup>b</sup> The Institute for Solid State Physics, The University of Tokyo, 5-1-5 Kashiwanoha, Kashiwa 277-8581, Chiba, Japan<sup>c</sup> Institut de Minéralogie et de Physique des Milieux Condensés, Université Pierre et Marie Curie Paris 6—CNRS, 140 rue de Lourmel, 75015 Paris, France<sup>d</sup> A.V. Nikolaev Institute of Inorganic Chemistry of Russian Academy of Sciences, Siberian Division, Novosibirsk 630090, Russia

## ARTICLE INFO

## Keywords:

- C. High pressure
- C. X-ray diffraction
- D. Electrical properties
- D. Phase transitions
- D. Transport properties

## ABSTRACT

The paper reports details of a high-pressure thermoelectric power (Seebeck effect) technique up to 40 GPa. Several different types of high-pressure cells with anvil insets are presented. The technique was applied for measurements of pressure dependence of the thermopower of several substances including elemental metals (lead, Pb; indium, In), cerium–nickel alloy, Ce–Ni and sulphur, S. Two peculiarities in the pressure dependences of the thermopower of CeNi were found and attributed to structural transformations, near  $\sim 5$  and  $\sim 10$  GPa. These transitions were confirmed in direct X-ray diffraction studies. Sulphur compressed to 40 GPa exhibited a hole type conductivity and the thermopower value was about  $\sim +1$  mV/K. Additionally, as an example of pressure calibration, the data on the electrical resistivity of zinc selenide, ZnSe, are given in a range of 0–23 GPa. These data suggest three possible scenarios of phase transitions from a rock salt (RS) high-pressure phase of ZnSe under decompression: RS  $\rightarrow$  zinc blende (ZB), RS  $\rightarrow$  cinnabar  $\rightarrow$  ZB, and RS  $\rightarrow$  wurtzite.

© 2010 Elsevier Ltd. All rights reserved.

## 1. Introduction

Transport properties carry information about the parameters of charge carriers and pressure-driven modification of an electron band structure, and thereby they can assist in clarification of pressure-induced changes in conducting materials. However, direct *in-situ* measurements of different transport properties under high pressure still remain challenging, and high-pressure transport investigations are basically limited to electrical resistivity. A series of pioneer studies on the electrical resistivity to 10–40 GPa (e.g. [1–6]) established phase transitions in many semiconductors and metals and thereby greatly promoted the high-pressure materials science.

High-pressure experiments are often carried out on a sample loaded inside a pressure transmitting medium (gases, liquids, gels, solid powders, and others) [7]; this provides a uniformity of pressure around a sample. However, a range of truly 'hydrostaticity' is limited by several GPa [8], and at higher pressures some pressure gradients on a sample may appear. Often, high-pressure transport techniques are miniaturizations or simple

adaptations of conventional ambient-pressure measurement schemes for utilization in a very limited working area; potentially they can progress following advances in nanotechnologies. Meanwhile, alternative approaches developed directly for high-pressure cells may operate better. For instance, an original method of measurement of the thermal conductivity at very high pressures and temperatures has been offered and verified in [9]. In [10] an original method of measuring the magneto-thermoelectric Nernst–Ettingshausen effects has been offered and tested on some elemental and binary compounds [11,12]. Notice that thermal transport experiments (e.g. thermoelectric, magnetothermoelectric, etc.) are more complicated than electrical ones, since one needs to additionally control the thermal flows. Thus, for instance, it makes it difficult to utilize any heat-conducting pressure-transmitting medium (gas, liquid, etc), as the heat distribution inside this media will confuse with the one inside the sample. Hence, there is a problem for high-pressure thermal measurements consisting in a search for acceptable compromise between an 'accuracy' of measurements and a 'quality' of pressure (pressure medium).

In this work we present details of the original approach for measurement of Seebeck effect (thermoelectric power) under high pressure and demonstrate its efficiency for a number of examples. Contrary to electrical resistivity, which is an integral effect of different electron bands, thermopower is a differential technique that makes it more sensitive to changes in electron

\* Corresponding author. Present address: Bayerisches Geoinstitut, Universität Bayreuth, Universitätsstraße 30, D-95447 Bayreuth, Germany.

E-mail addresses: [sergey2503@gmail.com](mailto:sergey2503@gmail.com), [sergey.ovsyannikov@uni-bayreuth.de](mailto:sergey.ovsyannikov@uni-bayreuth.de) (S.V. Ovsyannikov).

band structure. Another advantage of thermopower over electrical resistivity is that the former is insensitive to a sample's geometry. Measurement of Seebeck effect under high pressure is very important for several groups of tasks, for instance, as follows:

- (i) for a search for excellent high-pressure thermoelectric materials, i.e. materials that exhibit significant improvement in their thermoelectric power factors and figures of merit under compression. For instance, such effects were found in PbTe [13,14], Bi<sub>2</sub>Te<sub>3</sub> [15], Sb<sub>1.5</sub>Bi<sub>0.5</sub>Te<sub>3</sub> [16], HgTe [17,18], and in some others.
- (ii) for a careful examination of pressure-induced phase transitions and electron band structures of high-pressure phases. Thus, the thermopower revealed the high-pressure states with an electron type of conductivity in ZnTe and GaAs, which potentially could be related to some undetermined structures [19,20].
- (iii) for geophysical goals. If Seebeck coefficient of the basic earth-constitutive materials (spinel, magnesiowustite, silicates, etc.) is measured as a function of pressure and temperature, then one can construct a map of the conductivity types (*n*- and *p*-) in the Earth's interiors. Furthermore, one can infer a model of distribution of electrical voltages in the Earth. Also Seebeck effect appears to be useful for the estimation of Fe<sup>2+</sup>/Fe<sup>3+</sup> ratio in iron-rich minerals [21,22].

Thus, we report details of the high-pressure thermopower technique and relevant setups (Section 2). In Section 3 the applications are shown of the technique and setup for calibration of both pressure inside a high pressure cell (for example on ZnSe) and the thermopower (on examples of elemental pure metals, Pb and In). In Section 4 the results are given on the high-pressure thermopower of Ce–Ni and sulphur.

## 2. Experimental details

The principal schemes of anvil cells for measurement of Seebeck effect are shown in Fig. 1. We employ three different types of anvils as follows: (i) semi-concave anvils made of tungsten-carbide hard alloy or titanium carbide-nitride for a range up to 12 GPa (analogues of toroidal cells [23,24]) (Fig. 1a), (ii) flat anvils made of synthetic diamonds (conducting or insulating) for a range up to ~20–40 GPa (Fig. 1b), and (iii) bevelled anvils made of synthetic diamonds for a range up to ~60 GPa (Fig. 1c). Synthetic diamonds are characterised by a high resistivity to stresses and in a 'safe' pressure regime (i.e. for pressures below ~20 GPa) they are able to survive for many tens of cycles. The working diameters of the anvils (Fig. 1) vary from 0.2 to 1 mm. The cells with semi-concave anvils (Fig. 1a) employ bulk samples of typical sizes ~200–300 × 200–300 × 200–300 μm<sup>3</sup>, while in the diamond cells (Fig. 1b, c) the disk-shaped samples of a diameter ~100–300 μm and a thickness ~10–30 μm are loaded. The semi-concave cells (Fig. 1a) provide a quasi-hydrostatic compression [23,24]. In order to suppress axial components of pressure in the cells with flat anvils (Figs. 1b, c), a container's (gasket's) thickness in its central part should be much smaller than a working diameter of the anvils (for instance, in [25] a threshold ratio of ~0.055–0.057 separating quasi-hydrostatic contraction and the one with a non-zero axial component has been established).

The containers for samples are made from the lithographic stone (soft CaCO<sub>3</sub>-based material [7]) and they serve as both gaskets and pressure transmitting medium (Fig. 2). In measurement of thermopower, an upper anvil is heated (Fig. 1). Such an assembly seems to be almost ideal for thermoelectric measurements since (i) a uniform thermal flow goes exclusively through the bulk of the sample from an upper "hot" anvil to a lower "cold" one, and (ii) a container of the lithographic stone provides a good

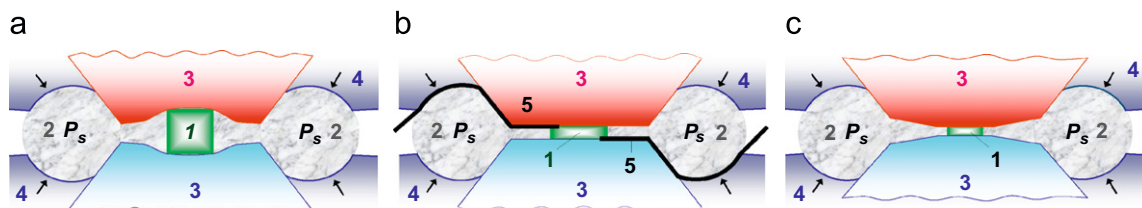


**Fig. 1.** Side views of high-pressure cells with different types of anvils: (a) anvils with a 'hole' operating up to 6–12 GPa, (b) conventional 'flat' anvils operating up to 20–40 GPa, and (c) bevelled anvils operating up to 60 GPa. **1** – a sample; **2** – a container made of lithographic stone [7]; **3** – the anvils; **4** – the supporting hard-alloy matrices (plungers), usually made of tungsten carbide; **5** – electrical probes to a sample on example of the cell in (b). A ring-like bulge of gasket **2** provides a supporting pressure  $P_s$  (up to 10 GPa) around the tips of the anvils; high quasi-hydrostatic pressure  $P$  is being created in the central part of the gasket around a sample.

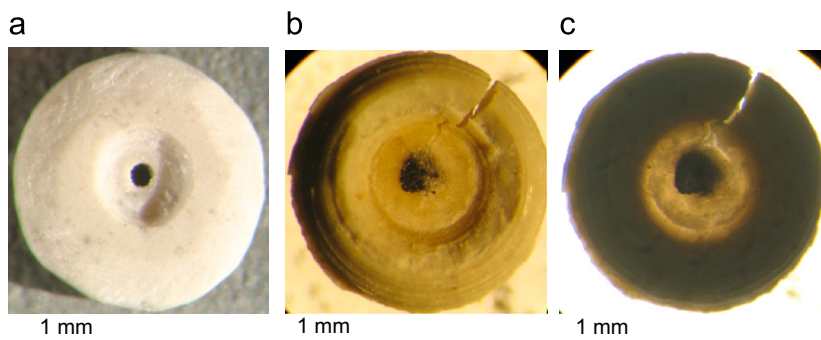


**Fig. 2.** Photographs of containers made of the lithographic stone (soft CaCO<sub>3</sub>-based material [7]): (a) a pristine container for a cell with a working diameter of the anvils  $d \sim 0.6$  mm; a central hole is of about 0.2 mm; (b, c) a recovered container with a sample (black circle) for a cell with  $d \sim 1$  mm. The lithographic stone becomes transparent under compression above ~20 GPa.

thermal isolation (Fig. 2). For measurement of thermoelectric voltage ( $U$ ) along a sample only one pair of electrical probes is required. For precise measurement a couple of thin Pt–Ag ribbons of  $\sim 5 \mu\text{m}$  in thickness is employed as electrical outputs to a sample [10,12,26]. Well-conducting synthetic diamond anvils also may be used as electrical outputs of a sample; in this case a possible small parasitic contribution to the thermopower value from the anvils themselves is beforehand determined by measurements of calibrated materials with close to zero thermopower, Pb, Au, Cu, Ag, In, etc. (see Section 3.2). A conventional four-probe resistivity method is also possible in these cells [27].

A temperature difference along a sample's thickness ( $\Delta T$ ) is determined from a temperature difference between the fixed points at the upper and the lower anvils; the latter is directly measured by means of the thermocouples. Calculations of a temperature distribution inside the 'anvils-container-sample' system performed in [28] for various thermal conductivity and thickness of a sample proved this method. For verification, several calibrated substances with the known thermopower values were measured, and after a comparison the corresponding small correction factors for  $\Delta T$  were extracted.

This approach permits comparative measurements of the thermopower in three regimes: (i) at fixed pressure under increasing and decreasing in a temperature difference  $\Delta T$ , (ii) at fixed  $\Delta T$  (or fixed density of a thermal flow  $q$ ) under variation in pressure, and (iii) in a non-stationary regime, i.e. under monotonic and almost continuous changing in both pressure and  $\Delta T$ . All three methods give the same results.

For measurement of a pressure dependence of the thermopower  $S$ , a cell is put in a cassette, which is introduced into an automated high-pressure setup (Fig. 3) [29]. Pressurization and decompression cycles in this setup are accomplished with assistance of an electromotor, i.e. almost continuous variation in pressure is provided. Applied force is *in-situ* measured by a digital dynamometer with resistive-strain sensors [28]. The pressure values inside the cells are determined are an uncertainty less than  $\sim 10\%$  from a calibration "stress-pressure" curve based on the

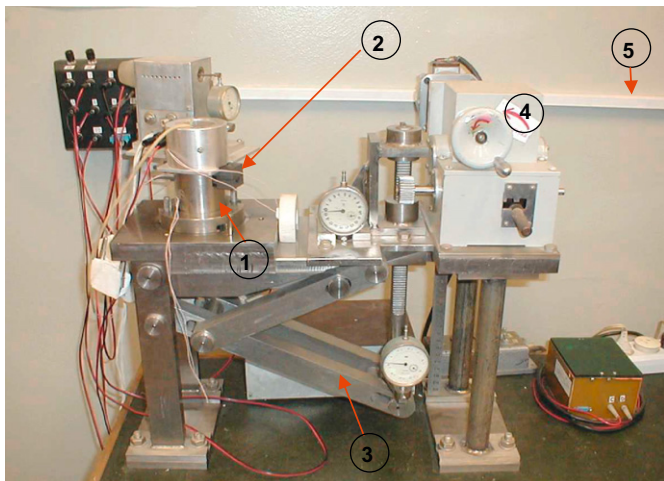


**Fig. 3.** A photograph of one of the automated portable high-pressure setups made of titanium alloy, which are utilized for measurements of pressure dependencies of the thermopower, the electrical resistivity, a temperature difference along micro-sample's thickness, and a sample's contraction under almost continuous variation in pressure. The setups produce stress about 3–5 tons. **1** – a pressure chamber, **2** – a cassette with a high-pressure cell loaded in the high-pressure chamber, **3** – a lever mechanism transmitting stress on the bottom of the pressure chamber (**1**), **4** – a reduction gear with the electromotor and handle drives, **5** – an electric cable for transmission of electrical signals from a sample and the setup to nanovoltmeters, which are related to a computer.

known and well-detectable pressure-induced transitions in Bi, PbS, PbSe, CdSe, ZnS, ZnSe, GaP and in other compounds [28]. An abruptness of some pressure-driven phase transitions, for instance, those in ZnSe (see Section 3.1), evidences the absence of significant pressure gradients around a sample.

The first thermopower study in a high pressure range ( $> 10 \text{ GPa}$ ) was performed using a similar cell [30]. At present there are only a few types of high-pressure cells for thermopower measurement, including the large-volume compressible capsules with a liquid media [31,32], DACs with a cross temperature difference [33–36], and some others [37].

### 3. Measurement of 'calibration' materials

#### 3.1. Zinc selenide (ZnSe): three scenarios of decompression from the rock salt phase?

Zinc chalcogenides (ZnTe, ZnSe and ZnS) exhibit a very abrupt 'insulator–metal' transition under pressure near 12–15 GPa (for example, [38]) and for this reason they are key materials for calibration of high-pressure cells beyond 10 GPa. Moreover, only in ZnTe this transition leads to a truly metallic phase, while those in ZnSe and ZnS are likely heavily doped semiconductors since they keep both the energy gaps approximately equalled to 1 eV [39,40] and are characterized by high thermopower values [38].

For the purposes of verification of 'stress-pressure' calibration curve in the diamond high-pressure cells (Fig. 1b, c) we measured the electrical resistivity of ZnSe across this 'insulator–metal' transition for many times and cycles. The basic transition scenario consists in a transformation from the ambient zinc blende (ZB) lattice to a rock salt (RS) one near  $\sim 13$ –15 GPa on pressurization, and near  $\sim 7$ –9 GPa on decompression (e.g. [40,41]). However, in a couple of studies [42,43] an intermediate cinnabar phase was detected; thus, for decompression a sequence was found as follows: RS  $\rightarrow$  cinnabar  $\rightarrow$  ZB, respectively, at 10.9 and 10.1 GPa [43]. Our results distinctly show three different scenarios for the decompression (Fig. 4). The curves #1 correspond to the 'typical' decompression scenario: RS  $\rightarrow$  ZB (Fig. 4). Curve #2 exhibits a gradual increase in the resistance below  $\sim 11 \text{ GPa}$ , and then its jump below  $\sim 6 \text{ GPa}$ . This could match well the following path: RS  $\rightarrow$  cinnabar  $\rightarrow$  ZB, if we take into account the fact that the known cinnabar phases (e.g. the one in ZnTe [19]) are semiconductors. Curve #3 shows a significant decrease of the transition pressure to an insulator phase (Fig. 4). By analogy with ZnS in which the transition pressures from an RS-structured high-pressure phase to the ambient ZB and wurtzite (WZ) ones were found to be, respectively,  $\sim 7$  and  $\sim 4 \text{ GPa}$  [44], we may propose that decompression of RS–ZnSe may also lead to a WZ lattice. No distinct features that could evidence the existence of other phases, e.g. predicted intermediate SC16 (simple cubic with 16-atom basis) lattice [45,46], were registered. Thus, the automated setup permitted the observation of several possible scenarios of phase transitions in ZnSe under pressure.

#### 3.2. High-pressure thermopower of lead and indium

Normally, metals have a low Seebeck coefficient and high magnitudes of thermal conductivity; the latter prevents generation of a temperature difference along a sample. For these two reasons accurate high-pressure thermopower measurement of metals is a complicated task. To examine the accuracy of our technique we chose two pure metals, namely, polycrystalline lead (99.9999%,  $S \sim -(1.1\text{--}1.3) \mu\text{V/K}$  [47,48]) and poly-crystalline

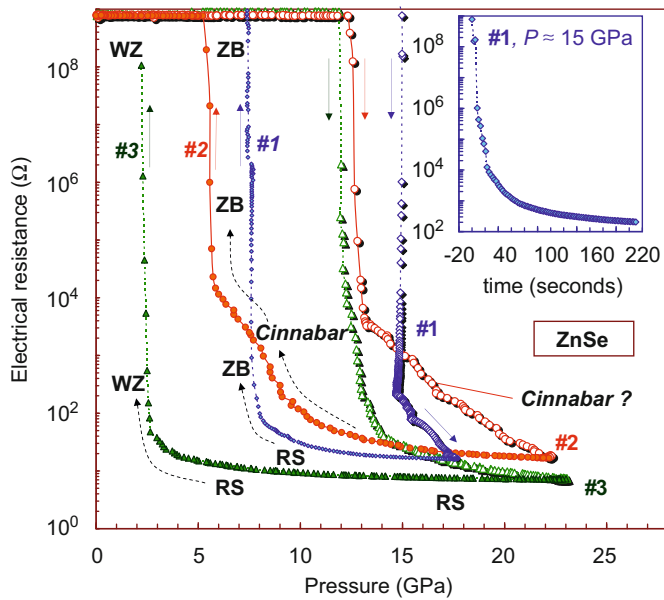


**Fig. 4.** The dependencies of the electrical resistance ( $R$ ) of ZnSe at 295 K on pressure ( $P$ ). #1, #2 and #3 correspond to different micro-samples cut from the same bulk single-crystalline ingot. The arrows show the direction of pressure variation. The decompression cycles of all the samples show different transformation paths: #1: rock salt  $\rightarrow$  zinc blende [38]; #2: rock salt  $\rightarrow$  cinnabar  $\rightarrow$  zinc blende; and #3: rock salt  $\rightarrow$  wurtzite [28]. The inset shows a time evolution of the electrical resistivity after the onset of the transition near 15 GPa in sample #1.

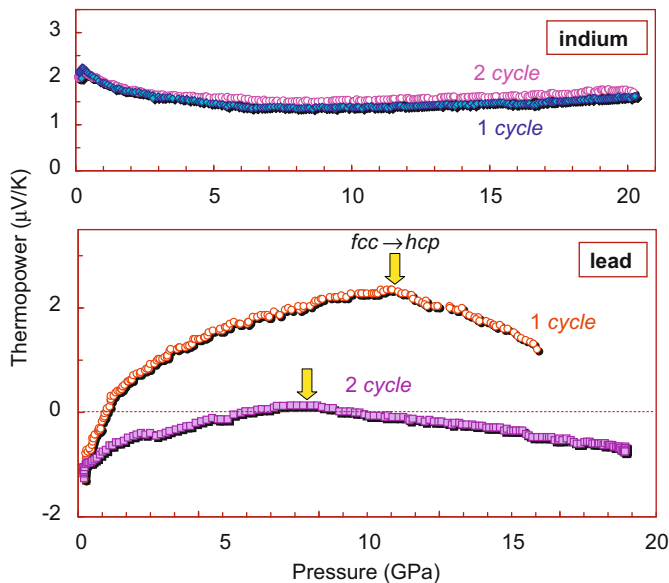


**Fig. 5.** The dependencies of the thermopower ( $S$ ) of indium (In) and lead (Pb) at 295 K on pressure for selected pressurization cycles. A kink near 14 GPa in the curves for lead was addressed to the known  $fcc \rightarrow hcp$  phase transition [49,50].

indium (99.99%,  $S \sim +2 \mu\text{V/K}$  [47]) and measured their thermopower up to 20 GPa (Fig. 5). One can see that the results obtained are in good agreement with the above ambient literature data [47,48]. These high-pressure thermopower data for metals serve for calibration of high-pressure cells in which the anvils serve as electrical probes to a sample. In such a case a high-pressure cell itself can bring a small parasitic contribution to a thermopower value, and testing measurements on metals permit ascertainment of its sign and value. Notice that for a conventional semiconductor with a thermopower value of about 100–300  $\mu\text{V/K}$  this small parasite contribution of the cell (normally it is less than  $\sim 4 \mu\text{V/K}$ )

may be disregarded. However, it should be taken into account in investigations of high-pressure metal phases whose thermopower values are sufficiently low.

The thermopower of indium did not show any bright peculiarities up to 20 GPa (Fig. 5). In pure metals the expression for the thermopower is as follows [49]:  $S = (\pi^2 k^2 T / (3e\eta)) \chi_i$ , where  $k$  is Boltzmann's constant,  $T$  is absolute temperature,  $\varepsilon$  is the electron energy,  $\eta = \varepsilon_F / (kT)$  where  $\varepsilon_F$  is the Fermi energy,  $\chi_i = -(\partial(\ln \rho) / \partial(\ln \varepsilon))_{\eta}$ , where  $\rho$  is the electrical resistivity. Pressure dependence of the thermopower reflects an effect of a volume ( $V$ ) contraction, and according to Ref. [49]  $d(\ln S) / d(\ln V) = -d(\ln \eta) / d(\ln V) + d(\ln \chi_i) / d(\ln V)$ , where the first contribution accounts for an influence of the Fermi energy variation, likewise for the second one—variations in the electron band structure and phonon spectrum [49]. For 'hard' electron bands the second contribution is equal to zero, and in the approximation of 'free electrons'  $d(\ln S) / d(\ln V)$  is estimated as  $\sim +2/3$  [49]. Below 1 GPa, this value is in a reasonable agreement with those experimentally determined in some alkali metals, such as Li (+0.43), Rb (+2.1), Na (+0.39), while this is not the case with K (−0.36) [49]. At higher pressures the  $d(\ln S) / d(\ln V)$  coefficients in the above-mentioned metals are subjected to changes [49], hinting that changes in the electron structure and phonon spectrum may not be disregarded. In the case of indium the thermopower slightly decreased with pressure to 7–8 GPa (Fig. 5), which corresponds to a small positive coefficient of  $d(\ln S) / d(\ln V)$ . At pressures higher than 7–8 GPa the trend is inverted (Fig. 5). Thus, one can infer that the thermopower value in indium results from a competition between the changes in the Fermi energy on the one hand and those in the electron band structure and phonon spectrum on the other hand. The thermopower values determined from the linear slopes of dependencies of a thermoelectric voltage on a temperature difference  $\Delta T$  along a sample's thickness taken at ambient and maximal pressures (Fig. 6) are  $\sim +2 \mu\text{V/K}$ , i.e. in good agreement

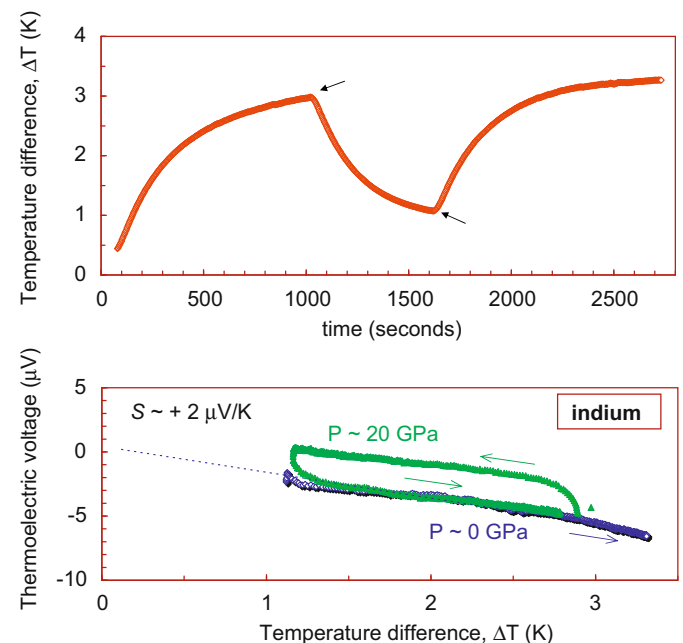


**Fig. 6.** Upper plot shows a typical time dependence of a temperature difference ( $\Delta T$ ) along a sample's thickness for heating–cooling–heating cycles at ambient pressure. The arrows point the switching on/off of an electrical heater that generates  $\Delta T$ . The lower plot shows a determination of the thermopower from a linear slope of a curve of a thermoelectric voltage on  $\Delta T$  at ambient and maximal pressures ( $\sim 20$  GPa, Fig. 5). The former was obtained before the pressurization on a heating cycle, and the latter—on a cooling–heating cycle.

with those above-discussed values obtained at pressurization at 'fixed'  $\Delta T$  (Fig. 5).

In the case of lead, a bend in the thermopower curve (i.e. inversion of the sign of a derivative  $d(\ln S)/d(\ln V)$ ) is observed near  $P \sim 13$  GPa (Fig. 5). It may be attributed to the sluggish  $fcc \rightarrow hcp$  phase transition [50,51]. On the second cycle this bend shifted to lower pressures (Fig. 5). The reduction in the transition pressure under pressure cycling normally could be explained by accumulation of pressure-induced defects in a sample's body; these defects supply additional nucleation sites and hence they can encourage phase transitions. Both the value and the sign of the thermopower of lead are determined by a competition between the two above-discussed contributions.

#### 4. Applications of the thermopower technique

##### 4.1. Pressure-induced phase transitions in CeNi

CeNi is the simplest representative of the family of  $CeNi_x$  ( $x=1, 2, 2.33, 3, 3.5, 4, 5$ ) heavy fermion alloys [52–60], and has the highest ambient thermoelectric power value among them,  $S \sim +27 \mu V/K$  [61,62],  $\sim +(21-27) \mu V/K$  [63],  $\sim +28 \mu V/K$  (in  $Ce_{0.8}Nd_{0.2}Ni$ ) [64], and only  $\sim +15 \mu V/K$  in Ref. [65]. CeNi adopts an orthorhombic lattice ( $Cmcm$  space group #63, CrB structural type). Under pressure application orthorhombic lattices, like CrB, TlI, GeS and others, were reported to possibly transform into a CsCl one [66–69], while some intermediate lattices are possible. The CrB structural type realizes in many metal alloys, for instance, in AgCa, NiB, VB, TaB, WB, ScAl, HfAl, AuTh, AuPr, AuCr, CeNi, CoTh, PtV, PrRh, CaSi, SrSi, BaSi, CaGe, CaSn, BaPb, and in many others. Thus, our interest was to probe the high-pressure behaviour of such CrB-structured alloys (on example of CeNi) in comparative thermopower and X-ray diffraction studies.

CeNi ingot was produced by melting in the argon atmosphere from pure Ce (99.99%) and Ni (99.99%) metals, taken in a 1:1 stoichiometric ratio. The ingot was then annealed at 973 K for six hours at 10 Pa in a quartz ampula. The crystal structure and chemical composition ( $Ce_1Ni_1$ ) of the alloys were determined in X-ray and neutron diffraction studies. In our sample the CrB structure has the following lattice parameters:  $a=3.785 \text{ \AA}$ ,  $b=10.545 \text{ \AA}$ ,  $c=4.355 \text{ \AA}$ . These values agreed well with data in [70,71]. The X-ray diffraction studies under pressure were performed on a station of the fourth channel of the VEPP-3 accelerator at the Budker Institute of Nuclear Physics of the Siberian Division of the Russian Academy of Sciences (Novosibirsk, Russia) in 0.3675- $\text{\AA}$  monochromatic synchrotron radiation [72]. Both the thermopower and X-ray diffraction studies were performed on several samples cut from the same ingot.

The ambient thermopower value of our CeNi samples was about  $S \sim 18.5 \mu V/K$  (Fig. 7a); this agrees with the other studies [61–65]. On the first pressurization cycle the pressure dependencies of the thermopower of CeNi samples (#1 and #2) exhibit distinct kinks near  $P \sim 4-5$  and  $\sim 9-11$  GPa (Fig. 7a). In the X-ray diffraction studies two structural transitions in CeNi were found by the appearance of new reflexes, near 4.5–5 GPa and around 10–12 GPa (Fig. 7b). Thus, the high-pressure thermopower technique proved its efficiency for a search for phase transitions in metallic alloys. Earlier, it was shown that the thermopower technique may be an effective tool for examination of pressure-driven transitions in lanthanides (Ce,Pr) [73,74].

Furthermore, the thermopower curves on the decompression cycles exhibit one return transition near 0.5–1 GPa (Fig. 7a). It appears to be related to a return transition from the second high-pressure phase to the first one (Fig. 7a). Thus, the thermopower data suggest that the first high-pressure phase is quenched.

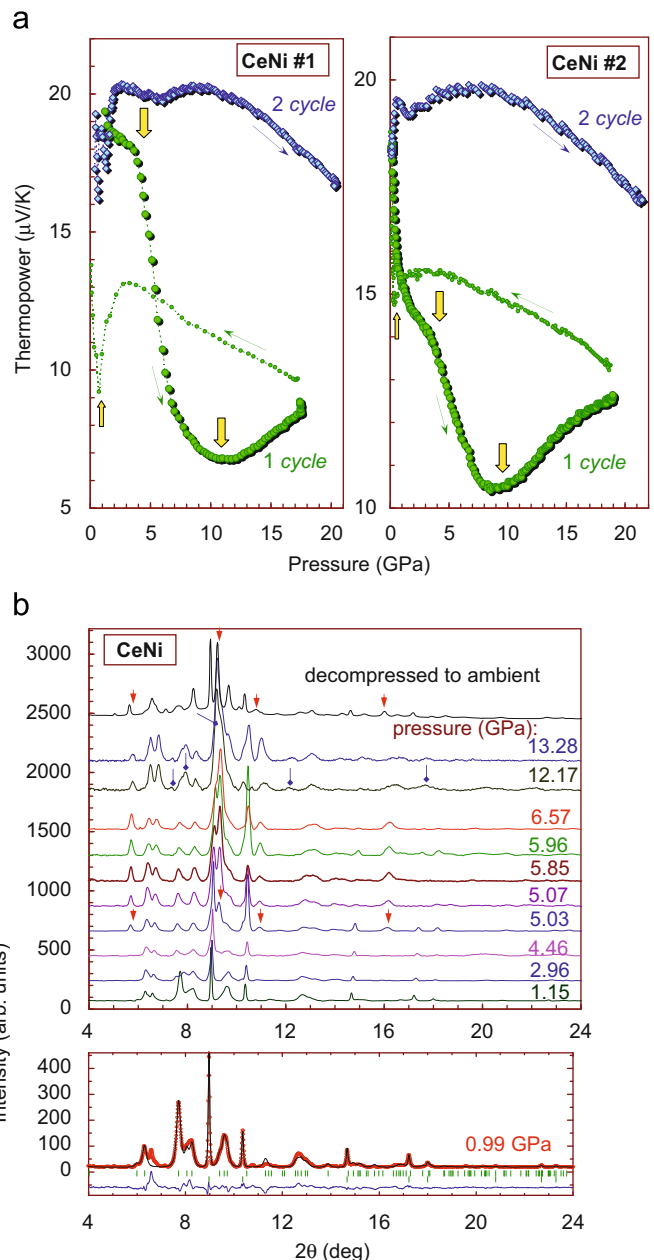


**Fig. 7.** The thermoelectric (a) and structural (b) properties of polycrystalline CeNi under pressure at 295 K. (a) #1 and #2 mark two different samples cut from the same ingot. The directions of pressure change are pointed by the arrows near the curves. The vertical arrows show the anomalies in the curves, which could be related to transitions. (b) The lower plot shows a Rietveld refinement of the X-ray diffraction patterns of CeNi at 0.99 GPa. The circles are the experimental data, the solid lines are the calculated profiles for the CrB structure (space group  $Cmcm$ ). The dashes show the reflectance position for the CrB structure (upper sets) and for Ag (lower sets). The lowermost curve is the difference between the experimental and the calculated profiles. The upper plot shows a pressure evolution of the patterns for selected pressures. Two phase transitions are seen at 5.03 and 12.17 GPa by the appearance of several new reflexes (marked by the arrows). The pattern taken after decompression evidences the persistence of a high-pressure phase.

The repressurization cycles drastically distinguish from the first ones (Fig. 7a), hinting at further phase transitions. X-ray diffraction pattern taken on a decompressed sample in fact shows the characteristic reflexes of the high-pressure phases (Fig. 7b) and thereby confirms the thermopower data.

In summary, this study on CeNi apparently demonstrates the potential of the technique of thermoelectric measurements. A detailed structural analysis of the discovered phases will be

performed in a separate work. One may notice that the CrB-structured metallic alloys containing valence-unstable Ce may behave in a more complicated manner than Ce-free ones. Thus, at low temperatures and pressures below 0.5 GPa some electronic transition was registered in CeNi and was attributed to pressure-effect on Ce atoms [57].

#### 4.2. Hole conductivity in sulphur at very high pressure

Direct measurements of the thermopower (supplying  $\Delta T$  and measurement of a thermoelectric voltage) of insulators are not possible because of a very high electrical resistivity. Indirect measurements, i.e. by means of thermoelectric current, are also difficult because of its small magnitude. At ambient conditions sulphur is a wide-gap insulator ( $E_g \sim 2.9$  eV). It was found that the gap decreases with pressure, hinting at the possibility of transport measurements at very high pressure. In order to determine the conductivity type in the high-pressure phases we compressed a single crystal of pure rhombic sulphur in a diamond cell (Fig. 1c). Under pressure the electrical resistivity of sulphur decreased, which permitted measurement of a thermoelectric current above 32 GPa (Fig. 8). Thus, the hole type of the conductivity and a value of the thermopower have been determined. In direct measurements above 36 GPa they were confirmed (Fig. 8). The decrease in the thermopower value with pressure (Fig. 8) agrees with a narrowing of the energy gap [75]. Thus, like the other members of VI Group, namely Te and Se [11,76], sulphur is also a semiconductor with the hole type of conductivity. For intrinsic semiconductors an expression for the thermopower may be written as follows [77]:  $S = -k/e \{ [(b-1)/(b+1)] E_g / (2kT) + [b/(b+1)] (r_n + 5/2) + [1/(b+1)] (r_p + 5/2) - (3/4) \ln(m_p/m_n) \}$ , where  $e$  is the electron charge,  $r_p$  and  $r_n$  are the scattering parameters of, respectively, holes and electrons,  $m_p$  and  $m_n$  are the effective masses of density of states of, respectively, holes and electrons, and  $b$  is a ratio of electron to hole conductivity. The largest first contribution determines a lowering of both the electrical

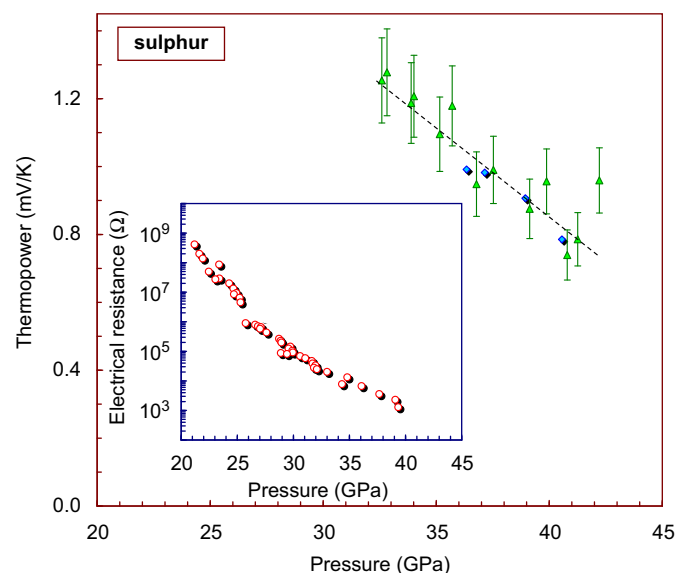


**Fig. 8.** The dependencies of the thermopower and of the electrical resistance of sulphur at 293 K on pressure. The blue rhombuses are the data determined from *in-situ* measured thermoelectric voltage ( $U$ ) and a temperature difference along a sample  $\Delta T$ ,  $S = U/\Delta T$ . The green triangles are the data determined from an *in-situ* measured thermoelectric current ( $I$ ) and an electrical resistance ( $R$ ),  $S = (IR)/\Delta T$ . For interpretation of the references to colour in this figure legend, the reader is referred to the web version of this article.

resistance and thermopower of sulphur with pressure (Fig. 8). The established dominant hole conductivity ( $b \approx 0$ ) may be related to several reasons, for instance: (i) higher mobility of holes than the one of electrons, and/or (ii) defect levels supply additional charge carriers (holes) or present themselves 'traps' for electrons.

## 5. Conclusion

The technique of measurement of the thermoelectric power (Seebeck effect) at high pressure has been reported. The accuracy of the technique has been verified in measurements of elemental metals, lead and indium. Application of the technique to CeNi revealed two phase transitions near 4–5 and 9–11 GPa, which were confirmed in direct X-ray diffractions studies. The technique permitted us to establish a hole type of conductivity in sulphur compressed beyond 30 GPa.

## Acknowledgements

The authors thank Dr. S.N. Naumov (IMP), Dr. V.I. Voronin (IMP) for the synthesis of the CeNi samples and their preliminary characterization, Ms. N.A. Shaydarova (IMP) for assistance in the thermopower measurements, Dr. A.Y. Likhacheva (Institute of Mineralogy and Petrography, Novosibirsk) for assistance in the X-ray diffraction studies under pressure, and Drs. B.N. Goshchitskii and A. Mirmelstein (IMP) for the useful comments on CeNi. The research was supported by the Russian Foundation for Basic Research (RFBR).

## References

- [1] P.W. Bridgman, Phys. Rev. 48 (1935) 893.
- [2] P.W. Bridgman, Proc. Am. Acad. Arts Sci. 72 (1938) 157.
- [3] P.W. Bridgman, Proc. Am. Acad. Arts Sci. 74 (1942) 425.
- [4] G.A. Samara, H.G. Drickamer, J. Phys. Chem. Solids 23 (1962) 457.
- [5] S. Minomura, H.G. Drickamer, J. Phys. Chem. Solids 23 (1962) 451.
- [6] A.S. Balchan, H.G. Drickamer, Rev. Sci. Instrum. 32 (1961) 308–313.
- [7] M.I. Eremets, in: High Pressure Experimental Methods, Oxford University Press, Oxford–New York–Toronto, 1996.
- [8] V.A. Sidorov, R.A. Sadykov, J. Phys.: Condens. Matter 17 (2005) S3005.
- [9] S.K. Saxena, G. Shen, P. Lazor, Science 264 (1994) 405.
- [10] V.V. Shchennikov, S.V. Ovsyannikov, JETP Lett. 74 (2001) 486.
- [11] V.V. Shchennikov, S.V. Ovsyannikov, Solid State Commun. 121 (2002) 323.
- [12] V.V. Shchennikov, S.V. Ovsyannikov, Solid State Commun. 126 (2003) 373.
- [13] S.V. Ovsyannikov, V.V. Shchennikov, Appl. Phys. Lett. 90 (2007) 122103.
- [14] Y. Wang, X. Chen, T. Cui, Y. Niu, Y. Wang, M. Wang, Y. Ma, G. Zou, Phys. Rev. B 76 (2007) 155127.
- [15] S.V. Ovsyannikov, V.V. Shchennikov, G.V. Vorontsov, A.Y. Manakov, A.Y. Likhacheva, V.A. Kulbachinskii, J. Appl. Phys. 104 (2008) 053713.
- [16] D.A. Polvani, J.F. Meng, N.V.C. Shekar, J. Sharp, J.V. Badding, Chem. Mater. 13 (2001) 2068.
- [17] V.V. Shchennikov, Phys. Solid State 42 (2000) 215.
- [18] X. Chen, Y. Wang, T. Cui, Y. Ma, G. Zou, T. Iitaka, J. Chem. Phys. 128 (2008) 194713.
- [19] S.V. Ovsyannikov, V.V. Shchennikov, Solid State Commun. 132 (2004) 333.
- [20] S.V. Ovsyannikov, V.V. Shchennikov, J. Phys.: Condens. Matter 18 (2006) L551.
- [21] N.F. Mott, in: Metal–Insulator Transitions, Taylor and Francis Ltd, London, 1974.
- [22] S.V. Ovsyannikov, V.V. Shchennikov, S. Todo, Y. Uwatoko, J. Phys.: Condens. Matter 20 (2008) 172201.
- [23] F.P. Bundy, Phys. Rep. 167 (1988) 133.
- [24] L.G. Khvostantsev, V.N. Slesarev, V.V. Brazhkin, High Pressure Res. 24 (2004) 371.
- [25] A.K. Bandyopadhyay, S. Chatterjee, E.S.R. Gopal, S.V. Subramanyam, Rev. Sci. Instrum. 52 (1981) 1232.
- [26] S. Kagoshima, R. Kondo, N. Matsushita, M. Higa, S.V. Ovsyannikov, N.A. Shaydarova, V.V. Shchennikov, A.Y. Manakov, A.Y. Likhacheva, Phys. Status Solidi (b) 244 (2007) 418.
- [27] S.V. Ovsyannikov, V.V. Shchennikov, S. Todo, Y. Uwatoko, High Pressure Res. 28 (2008) 601.
- [28] V.V. Shchennikov, S.V. Ovsyannikov, A.V. Bazhenov, J. Phys. Chem. Solids 69 (2008) 2315.

- [29] V.V. Shchennikov, S.V. Ovsyannikov, A.Y. Derevskov, V.V. Shchennikov jr, *J. Phys. Chem. Solids* 67 (2006) 2203.
- [30] I.M. Tsidi'kovskii, V.V. Shchennikov, N.G. Gluzman, *Sov. Phys. Semicond.* 17 (1983) 604.
- [31] L.G. Khvostantsev, V.A. Sidorov, *Phys. Status Solidi (a)* 82 (1984) 389.
- [32] D.T.K. Anh, T. Tanaka, G. Nakamoto, M. Kurisu, *J. Alloys Compd.* 421 (2006) 232.
- [33] D. Jaccard, E. Vargoz, K. Alami-Yadri, H. Wilhelm, *Rev. High Pressure Sci. Technol.* 7 (1998) 412.
- [34] B.T. Ferdin, N.V. Jaya, K. Anbukumaran, S. Natarajan, *Rev. Sci. Instrum.* 66 (1995) 5636.
- [35] D.A. Polvani, J.F. Meng, M. Hasegawa, J.V. Badding, *Rev. Sci. Instrum.* 70 (1999) 3586.
- [36] A. Segura, D. Errandonea, D. Martinez-Garcia, F.J. Manjon, A. Chevy, G. Tobias, P. Ordejon, E. Canadell, *Phys. Status Solidi (b)* 244 (2007) 162.
- [37] V. Vijayakumar, *J. Phys. Chem. Solids* 46 (1985) 17.
- [38] V.V. Shchennikov, S.V. Ovsyannikov, *Phys. Status Solidi B* 244 (2007) 437.
- [39] S. Ves, U. Schwarz, N.E. Christensen, K. Syassen, M. Cardona, *Phys. Rev. B* 42 (1990) 9113.
- [40] A.R. Goni, K. Syassen, *Semicond. Semimetals* 54 (1998) 247.
- [41] H. Karzel, W. Potzel, M. Kofferlein, et al., *Phys. Rev. B* 53 (1996) 11425.
- [42] M. Kobayashi, *Phys. Status Solidi (b)* 223 (2001) 55.
- [43] J. Pellicer-Porres, A. Segura, V. Munoz, J. Zuniga, J.P. Itie, A. Polian, P. Munsch, *Phys. Rev. B* 65 (2002) 012109.
- [44] S. Desgreniers, L. Beaulieu, I. Lepage, *Phys. Rev. B* 61 (2000) 8726.
- [45] A. Qteish, A. Munoz, *J. Phys.: Condens. Matter* 12 (2000) 1705.
- [46] R. Gangadharan, V. Jayalakshmi, J. Kalaiselvi, S. Mohan, R. Murugan, B. Palanivel, *J. Alloys Compd.* 359 (2003) 22.
- [47] C.L. Foiles, *Electrical Resistivity, Thermoelectrical Power and Optical Properties*, Landolt-Börnstein series, 15b, Springer-Verlag, 1985.
- [48] R.D. Barnard, in: *Thermoelectricity in Metals and Alloys*, Taylor and Francis, London, 1972.
- [49] F.J. Blatt, P.A. Schroeder, C.L. Foiles, D. Greig, in: *Thermoelectric Power of Metals*, Plenum, New York and London, 1976.
- [50] H.K. Mao, Y. Wu, J.F. Shu, J.Z. Hu, R.J. Hemley, D.E. Cox, *Solid State Commun.* 74 (1990) 1027–1029.
- [51] A. Kuznetsov, V. Dmitriev, L. Dubrovinsky, V. Prakapenka, H.P. Weber, *Solid State Commun.* 122 (2002) 125.
- [52] N. Marcano, D. Paccard, J.I. Espeso, J. Allemand, J.M. Moreau, A. Kurbakov, C. Sekine, C. Paulsen, E. Lhotel, J.C.G. Sal, *J. Magn. Magn. Mater.* 272 (2004) 468.
- [53] V.N. Lazukov, P.A. Alekseev, R. Bewley, R.S. Eccleston, K.S. Nemkovski, J.P. Sadikov, N.N. Tiden, *Physica B* 359 (2005) 245.
- [54] V.N. Lazukov, N. Marcano, N.N. Tiden, J.I. Espeso, J.C.G. Sal, P.A. Alekseev, R. Bewley, *Physica B* 378–80 (2006) 760.
- [55] H. Tsujii, E. Tanaka, T. Mamiya, S. Araki, R. Settai, Y. Onuki, *Physica B* 284 (2000) 1265.
- [56] D. Gignoux, F. Givord, R. Lemaire, F. Tasset, J. Less-Common Metals 94 (1983) 165.
- [57] D. Gignoux, J. Voiron, *Phys. Rev. B* 32 (1985) 4822.
- [58] G. Fillion, D. Gignoux, F. Givord, R. Lemaire, *J. Magn. Magn. Mater.* 44 (1984) 173.
- [59] A. Rudajeva, D. Vasylyev, O. Musil, *Physica B* 378–80 (2006) 758.
- [60] L. Nordstrom, M.S.S. Brooks, B. Johansson, *Phys. Rev. B* 46 (1992) 3458.
- [61] M.D. Koterlyn, R.I. Yasnitskii, G.M. Koterlyn, B.S. Morokhivskii, *Alloys Compd.* 348 (2003) 52.
- [62] R.V. Lutsiv, M.D. Koterlin, O.I. Babich, *Fiz. Tverd. Tela* 26 (1984) 1781.
- [63] J. Sakurai, H. Kamimura, T. Ohyama, Y. Komura, D. Gignoux, R. Lemaire, *J. Magn. Magn. Mater.* 70 (1987) 383.
- [64] I.S. Oliveira, K. Nishimura, N.J. Stone, Y. Isikawa, D. Zakoucky, D. Doran, *Phys. Rev. B* 49 (1994) 11886.
- [65] N.B. Brandt, V.V. Moshchalkov, N.E. Sluchanko, A.A. Gippius, T.M. Shkatova, *Fiz. Tverd. Tela* 27 (1985) 2484.
- [66] G.A. Samara, L.C. Walters, D.A. Northrop, *J. Phys. Chem. Solids* 28 (1967) 1875.
- [67] D. Becker, H.P. Beck, *Z. Kristallogr.* 219 (2004) 348.
- [68] H.P. Beck, G. Lederer, *Z. Anorg. Allg. Chem.* 619 (1993) 897.
- [69] P. Toledano, K. Knorr, L. Ehm, W. Depmeier, *Phys. Rev. B* 67 (2003) 144106.
- [70] A. Mirmelstein, E. Clementyev, V. Voronin, Yu. Akshentsev, D. Kozlenko, A. Kutepov, A. Petrovtsev, Yu. Zuev, *J. Alloys Compd.* 444–445 (2007) 281.
- [71] A. Mirmelstein, E. Clementyev, O. Kerbel, D. Kozlenko, Yu. Akshentsev, V. Voronin, I. Berger, *J. Nucl. Mater.* 385 (2009) 57.
- [72] V.V. Shchennikov, S.V. Ovsyannikov, A.Y. Manakov, A.Y. Likhacheva, A.I. Ancharov, I.F. Berger, M.A. Sheromov, *JETP Lett.* 83 (2006) 228.
- [73] S.V. Ovsyannikov, V.V. Shchennikov, B.N. Goshchitskii, *JETP Lett.* 81 (2005) 167.
- [74] S.V. Ovsyannikov, V.V. Shchennikov, B.N. Goshchitskii, *Mater. Sci. Eng. A* 462 (2007) 427.
- [75] H. Luo, S. Desgreniers, Y.K. Vohra, A.L. Ruoff, *Phys. Rev. Lett.* 67 (1991) 2998.
- [76] V.V. Shchennikov, *Phys. Solid State* 42 (2000) 641.
- [77] A.I. Ansel'm, in: *Introduction to Theory of Semiconductors*, Nauka, Moscow, 1978.